Jurnal Ilmu Fisika
Vol. 16, No. 1, March 2024, pp. 88–96
ISSN: 1979-4657 (Print); 2614-7386 (Online)
https://doi.org/10.25077/jif.16.1.88-96.2024

Jurnal Ilmu Fisika
Open Access

The Synthesized-Hydroxyapatite Powder from Anadara Granosa Shells using Deposition Time Method for Biomedical Applications

Sunardi Sunardi[1], Nidha Aulia Qurrata A'yun[1], Qorinah Wulan Dari[1], Jamrud Aminuddin[1], Bilalodin Bilalodin[1], Budi Praktino[2], Evi Yulianti[3], Agung Bambang Setio Utomo[4], Kartika Sari[1]

[1]Department of Physics, Faculty of Mathematics and Natural Science, Universitas Jenderal Soedirman, Jalan Dr. Suparno Karangwangkal, Purwokerto 53123, Indonesia
[2]Department of Mathematics, Faculty of Mathematics and Natural Science, Universitas Jenderal Soedirman, Jalan Dr. Suparno Karangwangkal, Purwokerto 53123, Indonesia
[3]National Research and Innovation Agency (BRIN), PRMM: Advanced Materials Research Center, KST BJ Habibie Serpong, Tangerang15314, Indonesia
[4]Department of Physics, Faculty of Mathematics and Natural Science, Universitas Gadjah Mada, Jalan Bulaksumur, Yogyakarta 55281, Indonesia

Article Info

Article History:

Received November 29, 2023
Revised February 02, 2024
Accepted February 07, 2024
Published online March 01, 2024

Keywords:

Hydroxyapatite
Anadara Granosa shells
XRD
FTIR
SEM

Corresponding Author:

Kartika Sari,
Email: kartika.sari@unsoed.ac.id

ABSTRACT

Hydroxyapatite (HAp) powder, one of the biomaterials derived from natural sources, could be used in biomedical applications. In this research, the synthesized-HAp powder from Anadara Granosa shells as raw materials had a high calcium carbonate content with variations in deposition time using the precipitation method. Variations of deposition time used were 0 (S0), 24 (S24), and 48 (S48) hours. Fourier Transform Infrared (FTIR), X-Ray Diffractions (XRD), and Scanning Electron Microscopy (SEM) were used to investigate the chemical structure, phase analysis, and morphology of the synthesized HAp powder. FTIR results of the S0, S24, and S48 showed that the functional groups PO_4^{3-}, CO_3^{2-}, and OH^- were formed at variations in the deposition time. The XRD results showed that the smallest of crystallite size of S48 was 26.03 nm, and the crystallinity degree of S24 was 38.74%. The grain dispersity of the synthesized-hydroxyapatite powder from SEM results were uniform, agglomeration, and spherical, irregular shape. The Ca, P, Mg, and Si compositions were shown in the synthesized-hydroxyapatite powder. The deposition time affects the synthesized-Hydroxyapatite (HAp) powder from the Anadara Granosa shell, and it is a potential raw material for biomedical applications.

1. INTRODUCTION

Biomaterials are materials sourced from natural or man-made materials that are used as substitutes for body tissues and can interact with the biological systems of the body (Sari & Yusuf, 2018). Synthetic biomaterials are used as a material for the healing or restoration of bone tissue and as an implantation technology in orthopedic surgery, so they are expected to increase the growth of cells in the replaced tissue (Ismail et al., 2021). One type of biomaterial is Hydroxyapatite (HAp) (Saharudin et al., 2017; Dhanaraj et al., 2018).

HAp ($(Ca_{10}(PO_4)_6(OH)_2$ is one of the most widely used types of apatite or calcium phosphate in the medical world because of its good compatibility and chemical and physical mineral content similar to human bones and teeth (Siswanto et al., 2019; Bulut et al., 2023; Kareem et al., 2024). HAp sources are often found in beef bones, clam shells, and crab shells (Afriani et al., 2020; Tjandra et al., 2023). The availability of HAp is a major problem for dentists as the primary users of this biomaterial. So far, HAp is still imported with a market price of one million rupiah per gram (Tanzi et al., 2019). HAp is the primary inorganic component of bone hard tissue and accounts for 60-70% of the mineral phase in bones (Fitriyana et al., 2019; Tjandra et al., 2023). HAp has biocompatibility, which is essential for biomedical applications (Dhanaraj & Suresh, 2018; Taji et al., 2022). HAp has a high calcium content, a hexagonal structure, and a constant or stable stable potassium phosphate crystalline phase. HAp has the advantages of being hollow, non-corrosive, active for tissues, and a stable compound in body fluids compared to other bone-forming compounds (Khoiriyah, 2018). HAp also has disadvantages, namely its brittle nature (Pu'ad et al., 2019; Zainol et al., 2022). HAp is found in animal bones such as fish and beef bones. HAp can be produced using various methods, including the hydrothermal method, continuous deposition, sol-gel method, solid-phase reaction, and electrophoretic deposition (Azis et al., 2015; Odusote et al., 2019; Kadir et al., 2022). HAp cannot be said to be a cheap biomaterial because the price per gram is one million rupiah. The availability of HAp is a primary matter for doctors, especially dentists (Tjandra et al., 2023).

The properties and synthesis methods of HAp have been studied by several researchers, however the process is expensive, complex, and time-consuming (Wu et al., 2023). Recently, there has been an increase in interest in creating high-performance hydroxyapatite powders by the natural resource synthesis of HAP. Nonetheless, research focusing on the simple and affordable production of HAp utilizing biowaste resources is still limited. Therefore, there is much promise for research on HAp synthesis from biowaste. The previous research has been carried out using abalone shells containing hydroxyapatite, which are suitable as biomaterial candidates with the most optimum variation of settling time, namely 48 hours based on crystal size, particle size, degree of crystallinity, and polydispersity (Mtavangu et al., 2022). The source of hydroxyapatite is Anadara Granosa shells because the primary content is calcium carbonate ($CaCO_3$) which reaches 59.87%. Calcium carbonate can be broken down into calcium oxide (CaO) and hydroxyapatite ($Ca_{10}(PO)_6(OH)_2$) (Pazarlioglu & Salman, 2019). Anadara Granosa shells are easy to find in Indonesia. Utilization of Anadara Granosa shells can increase the sale value of shellfish, reduce solid waste in the environment, and use natural materials to replace bone components (Almukarrama & Yusuf, 2019; Srichanachaichok & Pissuwan, 2023).

In this work, the synthesis and characterization of HAp based on Anadara Granosa shells with variations in deposition time using the precipitation method can be done. The characterization of HAp based on Anadara Granosa shells with variations in deposition time using 0, 24, and 48 hours was carried out to determine the functional groups using a Fourier-Transform Infrared Spectrometer (FTIR), the crystallite size, degree of crystallinity, and lattice strain using X-Ray Diffraction (XRD), and grain dispersity of the hydroxyapatite (HAp) powder using Scanning Electron Microscopy (SEM). The synthesized-HAp powder from Anadara Granosa shells is simple, low-cost, eco-friendly, and a potential raw material for biomedical applications.

2. METHOD

2.1 Materials and Tools

The main material used in producing HAp Powder in this research is Anadara Granosa Shells. To produce HAp Powder, Calcium Oxide (CaO) and $Ca(OH)_2$ (Calcium Hydroxide) must first be synthesized from Anadara Granosa Shells. After obtaining the synthesis results, Hydroxyapatite ($(Ca_{10}(PO_4)_6(OH)_2$) powder can be produced. The synthesis process requires the following materials: Aquades DM, Phosphoric acid (H_3PO_4) of about 85%, Sodium Oxide (NaOH), sieved paper, pH meter sheets, specimen sheets, and Aluminum Foil.

After the HAp powder is synthesized, the following process is the characterization process using FTIR, XRD, and SEM. The FTIR is the Shimadzu 8201 PC FTIR spectrophotometer, the XRD is the type Rigaku D/max 2500 V diffractometer, and the SEM is the type JEOL, JSM-6510LA.

2.2 Preparation Synthesis of CaO and $Ca(OH)_2$ powder from Anadara Granosa Shells

Figure 1 illustrates the synthesis process of CaO powder, which commenced by separating the shells of Anadara Granosa and thoroughly washing them until clean. The reaction of $CaCO_3$ to CaO can be seen in equation (1).

$$CaCO_3 \rightarrow CaO + CO_2 \quad (1)$$

Figure 1 Synthesis of CaO Powder from Anadara Granosa Shells**.**

The cleaned Anadara Granosa shells were subsequently dried, baked, and ground to obtain CaCO3 powder. This $CaCO_3$ powder underwent calcination for 3 hours to yield CaO powder. Following the calcination process, any remaining organic compounds in the sample were removed. The resulting Calcium Oxide was then ready for use. The synthesis of $Ca(OH)_2$ powder from Anadara Granosa Shells is depicted in Figure 2 as the subsequent step.

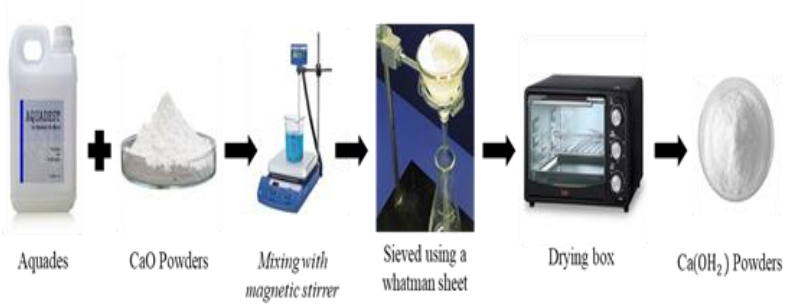

Figure 2 Synthesis of $Ca(OH)_2$ Powder from CaO powder of Anadara Granosa Shells**.**

Figure 2 depicts that the synthesis stage of $Ca(OH)_2$ powder was carried out by mixing CaO powder and distilled water using a hot plate magnetic stirrer and filtering to obtain a residue for one week. The residue is dried and becomes $Ca(OH)_2$ powder. The reaction of CaO to $Ca(OH)_2$ is as equation (2).

$$2CaO + 2H_2O \rightarrow 2Ca(OH)_2 \quad (2)$$

The formed-Calcium Hydroxide ($Ca(OH)_2$) will be used as a material for the synthesized-HAp powder.

2.3 Preparation Synthesis of Hydroxyapatite powder from Anadara Granosa Shells

The synthesis stage of HAp powder from Anadara Granosa Shells is shown in Figure 3. The reaction of $Ca(OH)_2$ to HAp powder is as in equation (3).

$$10Ca(OH)_2 + 6H_3PO_4 \rightarrow Ca_{10}(PO_4)_6(OH)_2 + 18H_2O \quad (3)$$

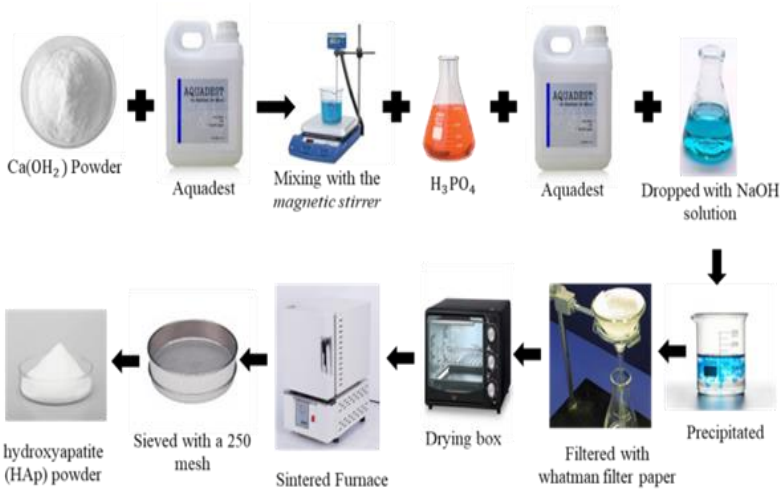

Figure 3 Synthesis of Hydroxyapatite Powder from $Ca(OH)_2$.

Figure 3 depicts the synthesis of HAp powders, which involved mixing $Ca(OH)_2$ powder and distilled water using a hot plate magnetic stirrer. Subsequently, H_3PO_4 mixed with distilled water was added dropwise to the mixture. The mixture was then adjusted to pH 10 by adding NaOH solution and precipitated according to two different setting times: 24 hours (S24) and 48 hours (S48). After precipitation, the resulting solution was dried, sintered, and sieved. The process of producing HAp powder using the precipitation method is illustrated in Figure 4.

Figure 4 HAp Powder from Anadara Granosa Shells**.**

2.4 Characterization of HAp Powder from Anadara Granosa Shells

The HAp powder was characterized using FTIR, XRD, and SEM techniques. FTIR spectrometry identified Ca-CO_3 functional groups. FTIR spectra of HAp Powder from Anadara Granosa Shells (S0, S24, and S48) were recorded at 1 cm^{-1} resolution in transmission mode (400-4000 cm^{-1}). Samples were mixed with KBr powder and pressed into pellets. Furthermore, XRD determined crystal size, crystallinity, and lattice strain, analyzing changes based on peak positions. XRD analysis utilized with Cu-Kα radiation (λ = 1.54060 Å), operating at 40 kV and 30 mA, with divergence slit/scattering slit settings and a 0.3 mm receiving one. Then, SEM assessed grain dispersity by capturing the surface of HAp Powder. Images from SEM were analyzed using Image J and Origin 10 software for sample morphology and grain dispersity assessment.

3. RESULTS AND DISCUSSION

The synthesized-HAp powder used a variation of settling time, namely 0 (S0), 24 (S24), and 48 (S48) hours, respectively. FTIR analysis is used to identify functional groups to determine PO_4^{3-}, and OH- groups in HAp powder. Result of FTIR spectra for HAp powder from Anadara Granosa shells with a variation of deposition time is shown in Figure 5 and Table 1.

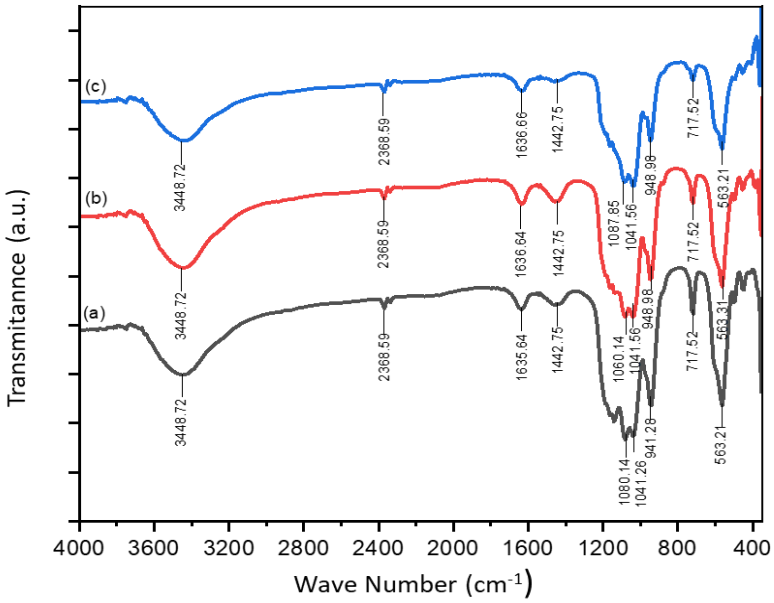

Figure 5 FTIR Spectra of the Synthesized-HAp powder (a) S0, (b) S24, and (c) S48**.**

Figure 5 and Table 1 present the FTIR spectra of synthesized-HAp powder from Anadara Granosa shells. The spectra reveal prominent chemical groups, notably CO_3^{2-}, OH-, and PO_4^{3-}. In the S0 spectrum, distinct characteristics are observed in both the functional group and fingerprint regions. The functional group region indicates the presence of the O-H functional group, while the fingerprint region suggests the presence of CO_3^{2-} and PO_4^{3-}. The phosphate group (PO_4^{3-}) exhibits bending at 563.21 cm^{-1}, typically observed in the 500 to 900 cm^{-1} range. Carbonate groups (CO_3^{2-}) are detected at wave numbers ranging from 717.52 to 941.26 cm^{-1}. Another phosphate group (PO_4^{3-}) is observed at 1080.14 cm^{-1}, indicating stretching. Additionally, stretching of the (OH-) group is detected at 3448.72 cm^{-1}.

Table 1 The Resulting Spectrum of FTIR on Hydroxyapatite.

No.	Functional groups	Wave Number (cm^{-1})			Vibration Types
		0 hour	24 hours	48 hours	
1.	PO_4^{3-}	563,21	563.21	563,21	Bending
2.	CO_3^{2-}	717,52	717.52	717,52	Bending
3.	CO_3^{2-}	941,26	948.98	948,98	Bending
4.	PO_4^{3-}	1080,14	1080.14	1087,85	Stretching
5.	C-O	1080,1–1041,56	1080,1–1041,56	1087,8–1041,56	Bending
6.	CO_3^{2-}	1442,75	1442,75	1458,18	Stretching
7.	C=O	1635,6–1442,75	1635,6–1442,75	1635,64	Stretching
8.	P^-	2368,5–2337,72	2368,59 – 2276	2368,5–2337,72	Bending
9.	O-H	3448,72	3448,72	3448,72	Stretching

For S24 and S48 spectra, similar functional groups are detected in both the functional group and fingerprint regions. The phosphate group (PO_4^{3-}) is observed at 1087.85 cm^{-1}, with no significant changes noted across time variations. Bending vibration occurs in the 700-900 cm^{-1} range, and carbonate groups (CO_3^{2-}) are also detected. Furthermore, a stretching vibration of the phosphate group (PO_4^{3-}) is observed at 1087.85 cm^{-1}, while the (OH-) group is detected at 3448.72 cm^{-1}. The intensity of HAp groups at wave numbers 3448 and 941 cm^{-1} suggests the presence of hydroxyl and phosphate groups. Comparing deposition time variations reveals no significant changes in the spectra pattern. The functional groups PO_4^{3-}, CO_3^{2-}, and OH- are consistently present in the HAp powder, indicating its composition. Although peaks are not sharply defined due to HAp's nature as an inorganic polymer, sharper peaks of PO_4^{3-} and OH- groups suggest higher absorption intensity (Rizkayanti & Yusuf, 2018; Mtavangu et al., 2022; Szterner & Biernat, 2022).

The intensity of absorption is directly proportional to the content of PO_4^{3-} and OH-. Higher absorption intensity indicates a higher content of PO_4^{3-} and OH-. Also, HAp exhibits good crystallinity growth, indicated by the sharper peaks of PO_4^{3-}. The analysis of precipitation time variations revealed that the phosphate group (PO_4^{3-}) exhibited a sharper peak at wave number 1087.85 cm^{-1} with a deposition time of 48 hours compared to other variations. This condition suggests that the 48-hour variation experienced better crystallinity growth. Since the functional groups CO_3^{2-} and PO_4^{3-} obtained from the FTIR results overlap, the value of the stretching vibration can be determined as a force constant.

XRD characterization of the synthesized-HAp powder from Anadara Granosa shells was conducted to determine phase structure, crystallite size, lattice strain, and crystallinity degree. The crystallite size was determined using the Debye-Scherer equation (1), the degree of crystallinity was measured using equation (2), and lattice strain was measured using equation (3). The diffraction peak width of the HAp plane was measured at half of the maximum intensity.

$$D = \frac{k\lambda}{\beta \cos\theta} \tag{1}$$

$$X_c = \frac{A_c}{A_c + A_a} \times 100\% \tag{2}$$

$$\varepsilon = \frac{\beta}{4 \tan\theta} \tag{3}$$

where D is the average crystallite size (nm), k is Scherrer constant (0.89), λ is the X-ray wavelength (1.5 A), β is the line broadening at FWHM (radians), θ is the Bragg's Angle (degrees), X_c is the degree of crystallinity, A_c is crystalline, and A_a is amorphous diffraction patterns, and ε is lattice strain.

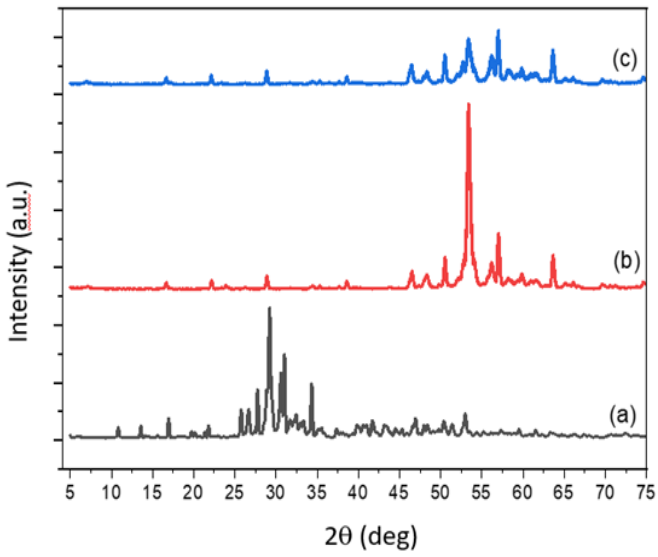

Figure 6 XRD Difractogram of HAp powder (a) S0, (b) S24, and (c) S48.

The X-ray diffraction (XRD) patterns of HAp powder derived from Anadara Granosa shells at different deposition times (S0, S24, and S48) are presented in Figure 6. In Figure 6(a), the peaks of S0 are observed at 2θ = 25 – 550. Moving to Figure 6(b), the peaks of S24 have shifted to the right side, with the highest peak appearing around 2θ = 53°. Finally, Figure 6(c) illustrates the reduced peaks of S48, concentrated around 2θ = 50 – 65°. The XRD phases of S0, S24, and S48 were identified as hexagonal crystal forms based on comparison with the standard Joint Committee on Powder Diffraction Standards (JCPDS Card No. 9 - 432). The crystallinity degree of S0, S24, and S48 is illustrated in Figure 7.

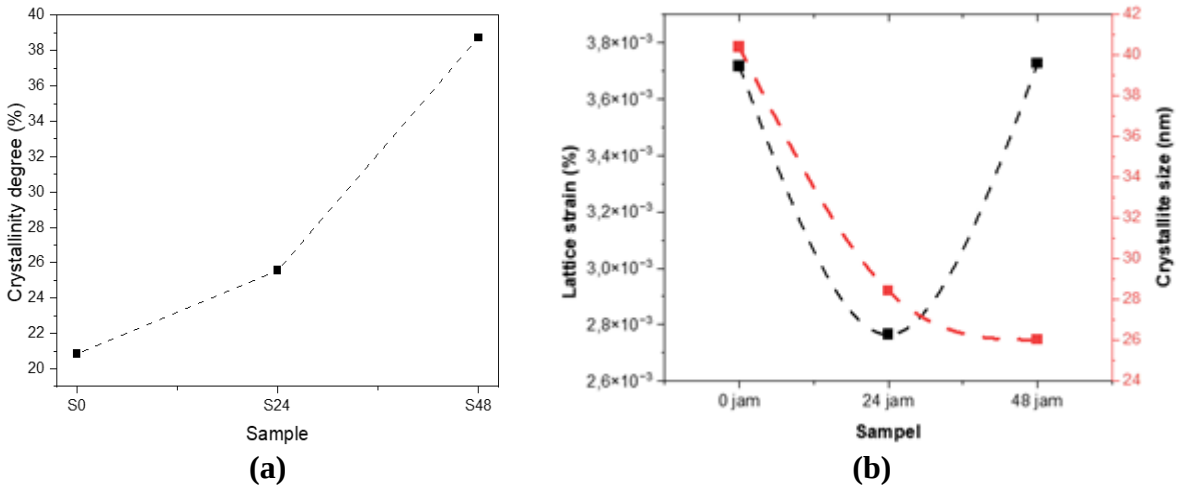

Figure 7 Cristalinitity Degree of HAp powder (a) and Crystallite Size and Lattice Strain of HAp Powder (b) of S0, S24, and S48

The crystallinity degree of HAp powder and the crystallite size and lattice strain of S0, S24, and S48 are examined (Figure 7). The crystallinity degree for S0, S24, and S48 is recorded as 20.84%, 25.57%, and 38.75%, respectively. The deposition time is observed to influence an increase in crystallinity degree due to the homogeneous dispersion of HAp powders. Conversely, the crystallite size and lattice strain of S0, S24, and S48 are measured as 40.40 nm, 28.43 nm, and 26.03 nm, respectively. The deposition time tends to decrease the crystallite size while significantly increasing the lattice strain. Longer deposition times result in smaller lattice strain values, as larger grain sizes lead to closer atom distances within the crystal, thereby reducing lattice strain.

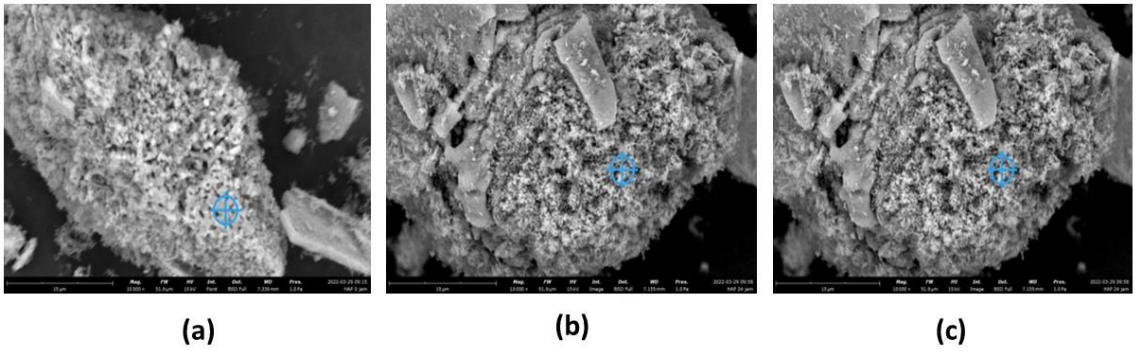

Figure 8 SEM pattern of Hydroxyapatite powder (a) S0, (b) S24, and (c) S48.

Consequently, the crystallite size of hydroxyapatite powder exhibits an inverse relationship with the lattice strain value. The obtained lattice strain indicates the occurrence of tensile strain within the crystal lattice. The relationship between the crystallite size of the synthesized-HAp powder and lattice strain is crucial in the welding process, where powder deformation causes a decrease in lattice strain value and an increase in crystallite size. Lattice deformation arises from lattice and crystal defects due

to plastic deformation resulting from atom movement and positional changes within the crystal structure, commonly called dislocation movement.

Figures 8 depict the surface morphology of S0, S24, and S48 derived from Anadara Granosa shells, exhibiting variations in deposition time. The grain dispersity of S0, S24, and S48 appears homogenous initially. However, as the deposition time increases, the homogeneity of grain dispersity diminishes. The results suggest highly agglomerated particles with relatively dispersed characteristics. The particles exhibit spherical-shaped morphology and are prone to agglomeration. Furthermore, the variation in deposition time can impact the material's particle size distribution, resulting in reduced empty spaces within the sample.

4. CONCLUSION

The results of the study can be concluded that the synthesis of hydroxyapatite from Anadara Granosa shells using the precipitation method with a variation of deposition time of the S0, S24, and S48 hours was successfully carried out. The functional groups present in the hydroxyapatite synthesis of the S0, S24, and S48 hours indicated the presence of PO_4^{3-}, CO_3^{2-}, and OH^- groups which indicated the presence of hydroxyapatite. Pure hydroxyapatite (S0) was not obtained due to the presence of CO_2 contaminants, so it was substituted with carbonate (CO_3^{2-}) in the hydroxyapatite crystal lattice. The hydroxyapatite crystal structure resulting from the precipitation method with variations in deposition time is obtained in the form of crystals. The crystallite size, crystallinity degree, and lattice wave of the S0, S24, and S48 hours resulted in a greater value. From XRD results the deposition time can affect the decreased crystallite size, and increased crystallinity degree, but significantly increase the lattice strain. The results of SEM are the grain dispersity of S0, S24, and S48 dispersed homogen. The research concluded that variation in deposition time has affected the surface morphology, cross-section morphology, and mechanical characteristics. HAp derived from Anadara Granosa shells is simple, low-cost, eco-friendly, and a potential raw material for synthesizing hydroxyapatite for biomedical applications.

ACKNOWLEDGEMENT

The authors would like to thank the financial support from the Ministry of National Education, especially the Bureau of Science Research and Universitas Jenderal Soedirman Grantee for supporting the “Riset Institusi Unsoed” of research in 2023.

REFERENCE

Afriani, F., Amelia, R., Hudatwi, M., & Tiandho, Y. (2020). Hydroxyapatite from natural sources: methods and its characteristics. *IOP Conference Series: Earth and Environmental Science*, *599*(1), 12055.

Almukarrama, & Yusuf, Y. (2019). Development carbonated hydroxyapatite powders from oyster shells (Crassostrea gigas) by sintering time controlling. *IOP conference series: materials science and engineering*, *546*(4), 42001.

Azis, Y., Jamarun, N., Zultiniar, Z., Arief, S., & Nur, H. (2015). Synthesis of hydroxyapatite by hydrothermal method from cockle shell (Anadara granosa). *J Chem Pharm Res*, *7*(5), 798–804.

Bulut, N., Kaygili, O., Hssain, A. H., Dorozhkin, S. V, Abdelghani, B., Orek, C., Kebiroglu, H., Ates, T., & Kareem, R. O. (2023). Mg-Dopant Effects on Band Structures of Zn-Based Hydroxyapatites: A Theoretical Study. *Iranian Journal of Science*, *47*(5), 1843–1859.

Dhanaraj, K., Kumar, C. S., & Suresh, G. (2018). Characterization of calcium oxide (CaO) derived from Perna viridis shell waste through solid state reaction. *J. Appl. Sci. Computation*, *5*(12), 658–665.

Dhanaraj, K., & Suresh, G. (2018). Conversion of waste sea shell (Anadara granosa) into valuable nanohydroxyapatite (nHAp) for biomedical applications. *Vacuum*, *152*, 222–230.

Fitriyana, D. F., Ismail, R., Santosa, Y. I., Nugroho, S., Hakim, A. J., & Al Mulqi, M. S. (2019). Hydroxyapatite synthesis from clam shell using hydrothermal method: A review. *2019 International Biomedical Instrumentation and Technology Conference (IBITeC)*, *1*, 7–11.

Ismail, R., Fitriyana, D. F., Santosa, Y. I., Nugroho, S., Hakim, A. J., Al Mulqi, M. S., Jamari, J., & Bayuseno, A.

P. (2021). The potential use of green mussel (Perna Viridis) shells for synthetic calcium carbonate polymorphs in biomaterials. *Journal of Crystal Growth*, *572*, 126282.

Kadir, L. A., Permana, D., & Azis, T. (2022). Sintesis dan Karakterisasi Bionano Hidroksiapatit (HAp) Secara Insitu Dengan Metode Hidrotermal. *Cokroaminoto Journal of Chemical Science*, *4*(2), 1–4.

Kareem, R. O., Bulut, N., & Kaygili, O. (2024). Hydroxyapatite biomaterials: a comprehensive review of their properties, structures, medical applications, and fabrication methods. *Journal of Chemical Reviews*, *6*(1), 1–26.

Khoiriyah, M. (2018). Sintesis dan Karakterisasi Bone Graft dari Komposit Hidroksiapatit/Kolagen/Kitosan (HA/Coll/Chi) dengan Metode Ex-Situ sebagai Kandidat Implan TulangSynthesis and Characteritation of Bone Graft from Hydroxyapatite/Collagen/Chitosan (HA/Coll/Chi) Composite By Ex-Situ Method As A Bone Implant Candidates. *Unesa Journal of Chemistry*, *7*(1).

Mtavangu, S. G., Mahene, W., Machunda, R. L., van der Bruggen, B., & Njau, K. N. (2022). Cockle (Anadara granosa) shells-based hydroxyapatite and its potential for defluoridation of drinking water. *Results in Engineering*, *13*, 100379.

Odusote, J. K., Danyuo, Y., Baruwa, A. D., & Azeez, A. A. (2019). Synthesis and characterization of hydroxyapatite from bovine bone for production of dental implants. *Journal of applied biomaterials & functional materials*, *17*(2), 2280800019836829.

Pazarlioglu, S., & Salman, S. (2019). Effect of lanthanum oxide additive on the sinterability, physical/mechanical, and bioactivity properties of hydroxyapatite-alpha alumina composite. *Journal of the Australian Ceramic Society*, *55*, 1195–1209.

Pu'ad, N. A. S. M., Koshy, P., Abdullah, H. Z., Idris, M. I., & Lee, T. C. (2019). Syntheses of hydroxyapatite from natural sources. *Heliyon*, *5*(5).

Rizkayanti, Y., & Yusuf, Y. (2018). Effect of temperature on syntesis of hydroxyapatite from cockle shells (Anadara granosa). *International Journal of Nanoelectronics and Materials*, *11*(2018), 43–50.

Saharudin, S. H., Shariffuddin, J. H., & Nordin, N. (2017). Biocomposites from (Anadara granosa) shells waste for bone material applications. *IOP Conference Series: Materials Science and Engineering*, *257*(1), 12061.

Sari, M., & Yusuf, Y. (2018). Synthesis and characterization of hydroxyapatite based on green mussel shells (perna viridis) with the variation of stirring time using the precipitation method. *IOP Conference Series: Materials Science and Engineering*, *432*, 12046.

Siswanto, S., Hikmawati, D., Aminatun, A., & Zamawi Ichsan, M. (2019). Hydroxyapatite-Collagen Composite Made from Coral and Chicken Claws for Bone Implant Application. *Materials Science Forum*, *966*, 145–150.

Srichanachaichok, W., & Pissuwan, D. (2023). Micro/Nano Structural Investigation and Characterization of Mussel Shell Waste in Thailand as a Feasible Bioresource of CaO. *Materials*, *16*(2), 805.

Szterner, P., & Biernat, M. (2022). The synthesis of hydroxyapatite by hydrothermal process with calcium lactate pentahydrate: the effect of reagent concentrations, pH, temperature, and pressure. *Bioinorganic Chemistry and Applications*, *2022*.

Taji, L. S., Wiyono, D. E., Karisma, A. D., Surono, A., & Ningrum, E. O. (2022). Hydroxyapatite Based Material: Natural Resources, Synthesis Methods, 3D Print Filament Fabrication, and Filament Filler. *IPTEK The Journal of Engineering*, *8*(1), 26–35.

Tanzi, M. C., Farè, S., & Candiani, G. (2019). *Foundations of biomaterials engineering*. Academic Press.

Tjandra, K. C., Novriansyah, R., Limijadi, E. K. S., Kuntjoro, L., & Hendrianingtyas, M. (2023). The effect of green mussel (Perna viridis) shells' hydroxyapatite application on alkaline phosphatase levels in rabbit femur bone defect. *F1000Research*, *12*, 631.

Wu, S.-C., Hsu, H.-C., Wang, H.-F., Liou, S.-P., & Ho, W.-F. (2023). Synthesis and Characterization of Nano-Hydroxyapatite Obtained from Eggshell via the Hydrothermal Process and the Precipitation Method. *Molecules*, *28*(13), 4926.

Zainol, I., Zainurin, M. A. N., Bakar, N. H. A., Jaafar, C. N. A., & Mudhafar, M. (2022). Characterisation of porous hydroxyapatite beads prepared from fish scale for potential bone filler applications. *Malaysian Journal of Microscopy*, *18*(2), 48–57.